Received: 5 December 2017 | Revised: 24 August 2018 | Accepted: 7 September 2018

DOI: 10.1111/ejn.14164

RESEARCH REPORT

WILEY EJN European Journal of Neuroscience FENS

Human posterior parietal cortex responds to visual stimuli as early as peristriate occipital cortex

Tamar I. Regev[1] | **Jonathan Winawer**[2] | **Edden M. Gerber**[1] | **Robert T. Knight**[3] | **Leon Y. Deouell**[1,4]

[1]Edmond and Lily Safra Center for Brain Science, The Hebrew University of Jerusalem, Jerusalem, Israel

[2]Department of Psychology and Center for Neural Science, New York University, New York, New York

[3]Helen Wills Neuroscience Institute and Department of Psychology, UC Berkeley, Berkeley, California

[4]Department of Psychology, The Hebrew University of Jerusalem, Jerusalem, Israel

Correspondence
Tamar I. Regev and Leon Y. Deouell, Edmond and Lily Safra Center for Brain Science, The Hebrew University of Jerusalem, Jerusalem, Israel.
Emails: tamaregev@gmail.com; leon.deouell@mail.huji.ac.il

Funding information
NIH, Grant/Award Number: R01MH111417; United-states Israel Binational Science Foundation, Grant Number: 2013070; Israel Science Foundation, Grant Number: 1902_2014

Abstract

Much of what is known about the timing of visual processing in the brain is inferred from intracranial studies in monkeys, with human data limited to mainly noninvasive methods with lower spatial resolution. Here, we estimated visual onset latencies from electrocorticographic (ECoG) recordings in a patient who was implanted with 112 subdural electrodes, distributed across the posterior cortex of the right hemisphere, for presurgical evaluation of intractable epilepsy. Functional MRI prior to surgery was used to determine boundaries of visual areas. The patient was presented with images of objects from several categories. Event-related potentials (ERPs) were calculated across all categories excluding targets, and statistically reliable onset latencies were determined, using a bootstrapping procedure over the single trial baseline activity in individual electrodes. The distribution of onset latencies broadly reflected the known hierarchy of visual areas, with the earliest cortical responses in primary visual cortex, and higher areas showing later responses. A clear exception to this pattern was a robust, statistically reliable and spatially localized, very early response, on the bank of the posterior intraparietal sulcus (IPS). The response in the IPS started nearly simultaneously with responses detected in peristriate visual areas, around 60 ms poststimulus onset. Our results support the notion of early visual processing in the posterior parietal lobe, not respecting traditional hierarchies, and give direct evidence for onset times of visual responses across the human cortex.

KEYWORDS
early visual processing, ECoG, electrocorticography, onset latency estimation

Abbreviations: AG, Angular gyrus; CAR, Common average reference; CI, Confidence intervals; CSD, Current source density; ECoG, Electrocorticography; ERP, Event-related potential; IPS, Intraparietal sulcus; ISI, Inter-stimulus interval; K, Koniocellular; LGN, Lateral geniculate nucleus; LIP, Lateral intraparietal; OLE, Onset latency estimate; PIP, Posterior parietal area; PN, Pulvinar nucleus; SC, Superior colliculus.

Edited by Prof. John Foxe. Reviewed by Semir Zeki and Steven Bressler.

All peer review communications can be found with the online version of the article.

1 | INTRODUCTION

Measuring the timing of neural responses in distinct cortical areas is important for understanding the network dynamics subserving sensory information processing in the brain. In particular, estimation of relative onset latencies can be used to test hierarchical relations and cortical connectivity. Specifically in the visual system, onset latencies of responses at various cortical and subcortical structures have been used

to map functional connectivity and distinguish streams of processing (Bullier, 2001; Chen et al., 2007; Ledberg, Bressler, Ding, Coppola, & Nakamura, 2007; Schmolesky et al., 1998; Schroeder, Mehta, & Givre, 1998). However, such measurements have been done primarily in laboratory animals.

Due to the difficulty of measuring human brain signals with both high spatial and temporal resolution, less is known about the precise spatiotemporal evolution of visual information processing in the human brain. In fMRI studies, the spatial resolution allows functional localization of specific parts of the visual system (such as V1, V2, etc.), using retinotopic mapping (Dumoulin & Wandell, 2008; Wandell & Winawer, 2011), but the temporal resolution is too low to study the latency of neural responses. Scalp EEG studies give good indication for the timing of processing (Foxe & Simpson, 2002). However, electrical measures on the scalp sum over an unknown number of anatomical sources, resulting in poor spatial resolution, as well as temporal smearing. Together with the ill-posed inverse problem of EEG source reconstruction, decomposing the EEG signal into its constituent components and localizing each component is a major challenge. MEG source reconstruction is similarly constrained by the inverse problem, but since magnetic fields are less distorted by the conductive medium than electric fields, localization is arguably more accurate than with EEG, while maintaining the same high temporal resolution. EEG and MEG studies have shown considerable variability in estimation of the onset time of visual responses (see summary in Shigihara, Hoshi, & Zeki, 2016). Some reported surprisingly early onsets in occipital cortex, as early as 25–30 ms (Inui & Ryusuke, 2006; Inui, Sannan, Miki, Kaneoke, & Kakigi, 2006; Moradi et al., 2003; Shigihara & Zeki, 2013, 2014), or in some cases even at 10–15 ms post onset (Shigihara et al., 2016). As previously argued (Shigihara et al., 2016), it is hard to compare absolute onset times between studies because onset times are affected significantly by the luminance, contrast, spatial frequency, size and location in the visual field of the stimuli. Rather, the relative latencies are most directly interpretable. The results of studies by Zeki and colleagues (Ffytche, Guy, & Zeki, 1995; Shigihara & Zeki, 2013, 2014; Shigihara et al., 2016), suggested parallel activation of V1 and peristriate cortex (i.e., with no lag), although due to the limitation of the method the precise location of the early activity could not be determined.

Here, we present an estimation of onset latencies of visually evoked responses across the posterior human cortex using electrocorticographic (ECoG) recordings, having the advantage of both spatial and temporal high resolution, in a single human patient requiring surgery for intractable epilepsy. The patient went through presurgical evaluation that included functional MRI followed by implantation of subdural electrodes covering various posterior cortical areas. We examined the spatio-temporal progression of visual responses in the cortex and examined the degree to which they abide by the established streams of processing. For that aim, we developed a statistical method for assessment of onset latencies in continuous signals using bootstrapping of baseline activity.

2 | MATERIALS AND METHODS

2.1 | Patient

The patient, who suffered from intractable epilepsy, was hospitalized for presurgical evaluation at the Stanford Medical Center. As part of this clinical procedure, the patient was implanted with subdural electrodes, to allow a more precise localization of the epileptic focus, so that it can be subsequently surgically removed. The number and location of the electrodes was determined solely based on clinical needs, and, before electrode implantation, the patient signed an informed consent to participate in our experiment. All procedures performed in this study were approved by the UC Berkeley Committee on Human Research and corresponding IRBs at the clinical recording site. The patient was a right handed, 45 years old male, English speaking, with normal intellectual abilities and no psychiatric or visuospatial abnormalities, as revealed by standard presurgical evaluation.

2.2 | Stimuli

The stimuli consisted of grayscale pictures of four categories; human faces, watch faces, drawings of everyday objects and pieces of clothing, which were the target stimuli. The categories of visual images served the purpose of another experiment and are largely ignored in this study focusing on early visual areas. The stimuli were 5.4 cm^2 on the background of a black 34.4 × 19.3 cm LCD screen (refresh rate 60 Hz), located about 65 cm away from the subject's eyes. Hence, the stimuli subtended about 4.6° of visual angle, in the centre of the visual field. The experiment was run under normal hospital room lighting.

2.3 | Procedure

The patient was half seated in his hospital bed with the laptop computer used to present the stimuli placed on a table suspended above (but not touching) his legs. The experiment was controlled by Eprime 2 running on Windows XP (Microsoft, Inc.) operating system. The position of the laptop allowed the patient to press the space key on the keyboard to indicate target detection. A photodiode on the bottom screen corner detected a bright rectangle which was presented on the screen together with the image. The bright rectangle was completely covered by the photodiode unit so that it was invisible to the subject. The signal from the photodiode was recorded alongside the EEG and later used to create stimulus triggers. The identity of each stimulus was recorded by Eprime and later merged with the triggers

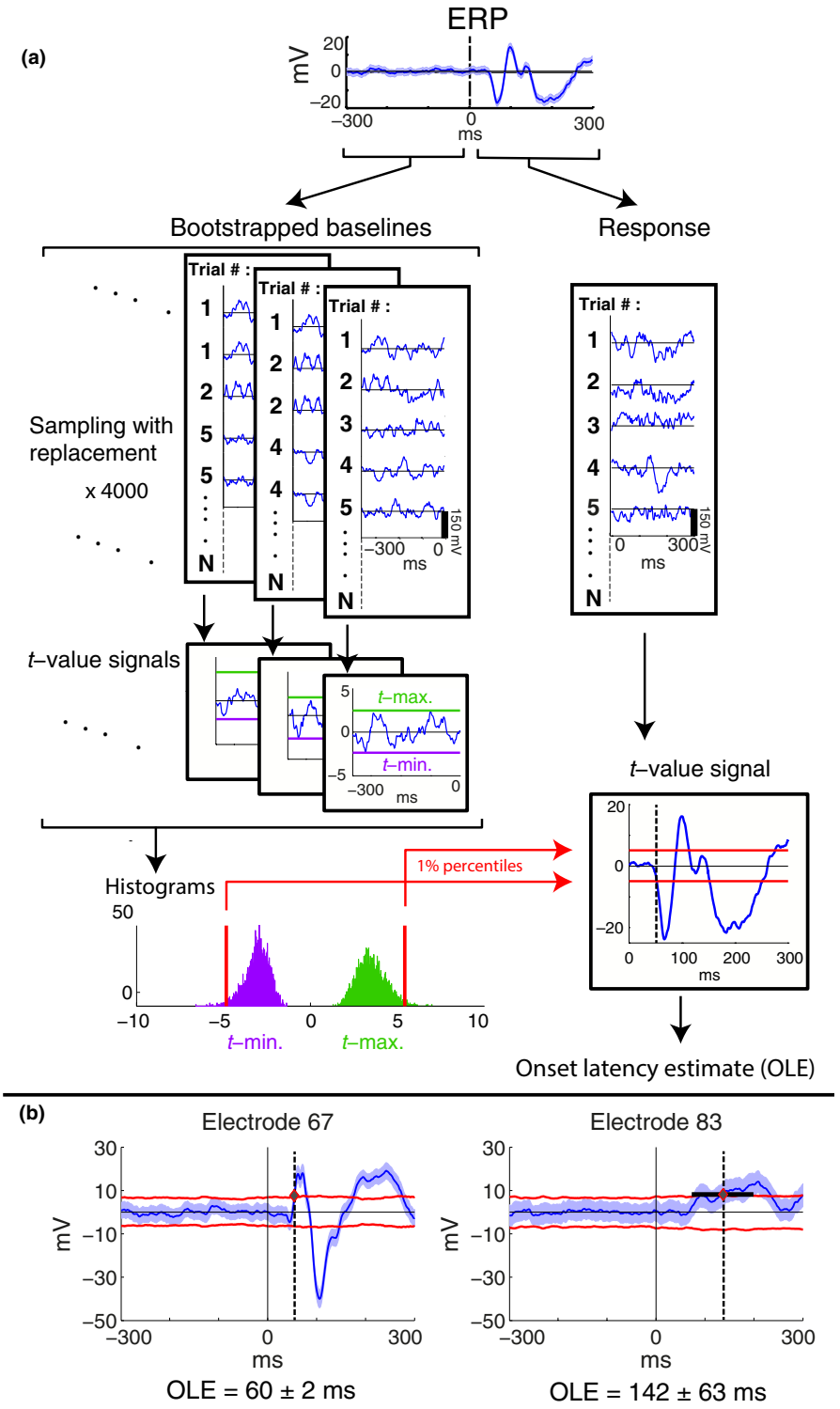

FIGURE 1 Illustration of the onset latency estimation method. (a) Calculation of an onset latency estimate (OLE) for a specific electrode via bootstrapping over the baseline trials, construction of empirical distributions of maximal and minimal *t*-values, and using the 0.01 percentile values as thresholds for the response t-value signal (see Section 2.10). (b) Estimation of temporal error of the OLE. Examples of specific electrodes having small or large temporal errors (left and right, respectively). Shaded blue area is 99% confidence interval around the mean. Red lines are the translation of the constant *t*-value thresholds back to the voltage domain, multiplying by the instantaneous standard error (see Section 2.10 for detailed explanation). Electrode numbers are specified in Figure 2. [Colour figure can be viewed at wileyonlinelibrary.com]

extracted from the photodiode channel. The lag between the onset of stimulus in the middle of the screen and that of the rectangle in the bottom-right corner of the screen was 5 ms, as measured using an analog oscilloscope after the experiment. This delay was taken into account in the analysis.

During the experiment, the patient was required to press the space key whenever he detected a piece of clothing (nearly 10% of stimuli). The experiment consisted of 8 blocks of 86 visual images mixed across the nontarget categories with equal shares. The duration of stimuli was 300, 600, 900, 1,200 or 1,500 ms, with equal probabilities. The variable durations served the purpose of another experiment (Gerber, Golan, Knight, & Deouell, 2017) and are largely ignored in the present study focusing on onset responses.

The order of the stimuli and durations were quasi-random. Interstimulus intervals (ISI) were between 600, 900, 1,200 or 1,500 ms, randomly distributed. Before the experiment started the patient was presented with a sample of the targets, and with a few practice trials, which were not recorded. In total, 688 stimuli were presented during the experiment.

2.4 | ECoG recording

The patient was implanted with 112 subdural electrodes covering areas of the occipital, parietal and temporal cortices of his right hemisphere. The electrodes (AdTech Medical Instrument Corp.) were 2.3-mm in diameter, and arranged in either 2D grids or 1D strips. Neighbouring electrodes were ~0.5–1 cm centre-to-centre apart from each other within a single grid or strip. The EEG signal was recorded with a Tucker-Davis Technologies (TDT) recording system at a sampling rate of 3,051.76 Hz, with an online 0.5 Hz high-pass filter.

2.5 | Electrode localization

Electrode locations were identified manually using BioImageSuite (www.bioimagesuite.org) on a postoperative Computed Tomography (CT) scan co-registered to a preoperative MR scan using the FSL software package (Jenkinson, Bannister, Brady, & Smith, 2002; Jenkinson & Smith, 2001). Individual subjects' brain images were skull-stripped and segmented using FreeSurfer (http://surfer.nmr.mgh.harvard.edu). Localization errors driven by both co-registration error and anatomical mismatch between pre and postoperative images were reduced using a custom procedure which uses a gradient descent algorithm to jointly minimize the squared distance between all electrodes within a single electrode array/strip and the cortical pial surface (Gerber et al. 2017; see Dykstra et al., 2012 for a similar procedure). In contrast to methods that only attempt to correct individual electrodes' position in relation to the pial surface, this method preserves the original array topography, thus providing a more reliable estimate of actual electrode positions. A related method (Hermes, Miller, Noordmans, Vansteensel, & Ramsey, 2010) was shown to localize electrodes to within 2–4 mm based on ground truth measures from intraoperative photography. We report the MNI coordinates of electrode 34 (see Section 3.2 'Very early visual response at posterior intraparietal sulcus'), based on surface registration to an MNI152 standard-space T1-weighted average structural template image.

2.6 | Co-registration with retinotopic mapping

Retinotopic mapping was performed preoperatively, as described in detail in a prior publication involving the same patient (Winawer et al., 2013; sections 'Stimuli for fMRI Experiments' and 'Anatomical and Functional MRI'). In brief, the patient was presented with a drifting checkerboard contrast pattern revealed within a moving bar aperture during nine 3.5-min scans. The functional data were co-registered to a whole-brain T1-weighted image ($1 \times 1 \times 1$ mm), which was segmented into grey and white matter, using Freesurfer's autosegmentation tool. The autosegmentation produces a cortical ribbon for each hemisphere, and the functional time series were resampled to the cortical ribbon via trilinear interpolation. Population receptive field models were solved on this resampled data, and model parameters—polar angle and eccentricity—were visualized on the cortical surface. Retinotopic maps were identified on the cortical surface following previous definitions of visual field maps and their boundaries (Wang, Mruczek, Arcaro, & Kastner, 2014; Winawer, Horiguchi, Sayres, Amano, & Wandell, 2010).

2.7 | Data analysis

The analysis was performed using Matlab software (The Mathworks Inc., Natick, MA) versions 2013b or 2016b, (yielding the same results) running on a Windows-based computer. The analysis steps are listed below.

2.8 | Preprocessing

Ten electrodes that were diagnosed clinically by the neurologist (Dr. Josef Parvizi) as including epileptic activity were ignored. The ongoing data was further reviewed by authors RTK and LYD and six more electrodes were ignored due to repeated electrical arteifacts. For the remaining electrodes, temporal periods in which epileptic activity or other occasional artefacts were observed anywhere were excluded from the analysis across all electrodes.

The data were downsampled to 1,000 Hz, and the 60 Hz oscillation caused by US electricity system was filtered out using a notch filter version that was developed in our lab (Keren, Yuval-Greenberg, & Deouell, 2010), which mainly removes the ongoing oscillatory component, with less effect on transients. We used common average reference (CAR)—a point-by-point average of all electrodes except for the epileptic and artifact-laden ones, or the current source density (CSD) local reference, as explained below in Section 2.11 'Current source density (CSD) estimation'.

2.9 | Event-related potentials (ERPs)

Since we were interested in the onsets of early visual responses irrespective of visual category or stimulus duration, the data was segmented to epochs lasting 600 ms, starting 300 ms before and ending 300 ms after stimulus onset. The baseline mean of the 300 ms preceding stimulus onset in each

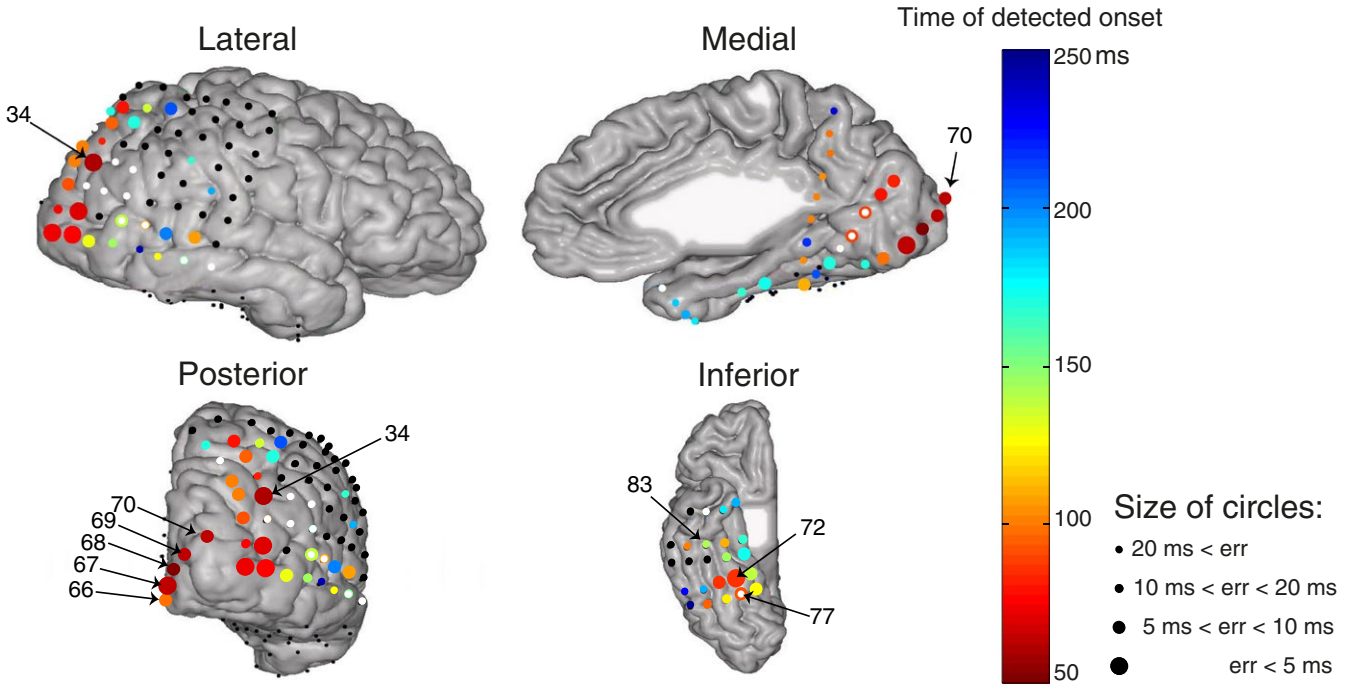

FIGURE 2 Significant visual onset latencies in all electrodes. Four views of the same brain are presented. The colour of the circles denotes the timing of the estimated onsets (see colour bar). The size of the circles denotes the temporal error estimates (see Section 2.10, 'onset latency estimation'): larger circles indicate more reliable estimates (smaller temporal errors; see legend). White dots indicate electrodes that were labelled as epileptic or with other electric artifacts. However, we looked for onset latencies of the bad electrodes as well, and if a significant onset was found, the coloured circle was placed under the white dot (e.g., electrode 77). Black dots indicate electrodes for which no significant onset was detected. Numbers are indicated here for electrodes that are explicitly mentioned in the text. For a full illustration of electrode numbers, see supporting information, Section 1. Note that some electrodes appear in more than one view, however their onsets and/or numbers might appear in some of the views, e.g., the onsets of inferior electrodes are not indicated in the posterior view. Common average reference (CAR). For a dynamic depiction of activation over time see supporting information Movie S1. [Colour figure can be viewed at wileyonlinelibrary.com]

trial was subtracted from each time point of the segment, and all nontarget trials (excluding artefacts) were averaged to calculate event-related potentials (ERPs) per electrode. The ERPs thus consisted of 569 trials.

2.10 | Onset latency estimation

To determine the first time point in which the ERPs significantly depart from baseline activity, we calculated the point-by-point one-sample t-value (against zero) across the trials per each electrode - $T_{\bar{V}(t)} = \frac{\bar{V}(t)}{S.E(\bar{V}(t))}$, whereas $\bar{V}(t)$ is the instantaneous average voltage across trials, and $S.E(\bar{V}(t))$ is the instantaneous standard error across trials. To determine a threshold t-value, we used a bootstrapping procedure over the 300 ms prestimulus baseline trials, which provided a distribution of expected t values under the null hypothesis of no response (Figure 1a). The bootstrapping procedure consisted of generating 4,000 different groups of $n = 569$ trials, by sampling with replacement from the original group of n baseline trials (see Figure 1a). The number 4,000 was determined such that increasing it did not change the final onsets, up to 1 ms. For each group of n bootstrapped trials, a baseline surrogate *t*-statistic signal (against 0, see formula above) was calculated point-by-point during the −300 to 0 prestimulus periods, and the maximal and minimal values of the t-statistic signal were noted. Histograms of the frequency distribution of maximal and minimal surrogate t-statistic values were generated for each electrode and the right and left 1% percentiles of the distribution were used as negative and positive thresholds for the actual response t-statistic signal, respectively (see Figure 1a). The onset latency estimate (OLE) for each electrode was determined as the first time-point at which the true t-value signal of the response (0–300 ms) passed either the high or the low threshold t-values for that electrode. Consequently, the equivalent alpha level was 0.02. Next, in order to compute a temporal error for the OLE, the *t*-value thresholds were converted back to voltage by multiplication of the constant *t*-value threshold by the instantaneous standard error of the voltage at each time point of the response trials. The temporal error margin was determined as the interval surrounding the OLE, in which the voltage threshold was within the 99% confidence interval (CI) around the ERP mean (i.e., the threshold was smaller than ERP + CI/2 or larger than ERP – CI/2). The temporal error was calculated as half of the length of this interval (see Figure 1b). Figure 1 illustrates the onset latency estimation procedure.

2.11 | Current source density (CSD) estimation

Due to volume conduction, the activity measured in a given electrode may reflect neural activity that is remote from the location of the electrode. To mitigate the effect of volume conduction, we also used CSD to estimate onset latencies (Carvalhaes & de Barros, 2015), which effectively applies a high-pass spatial filter to the voltage measurements. Due to the nature of volume conduction, activity conducted from far away sources should be quite similarly measured by adjacent electrodes. In contrast, local sources will be measured much more strongly by the electrode near the source, and the measured activity will drop sharply in nearby electrodes. The current source density map thus filters out widespread activity, which is suspect of being conducted from remote sources, and highlights local current sources.

The CSD is inversely proportional to the Laplacian of the voltage field: $\mathrm{CSD} = -\nabla^2 V$. It can be estimated easily by subtracting a local reference for each electrode (Butler et al., 2011; Hjorth, 1975; Schroeder et al., 1998). Effectively, the average voltage of the four or two neighbouring electrodes is subtracted for each electrode residing on a 2D grid or 1D strip, respectively:

$$\mathrm{CSD}^{\mathrm{grid}}_{i,j} \approx V_{i,j} - \frac{V_{i+1,j}+V_{i-1,j}+V_{i,j+1}+V_{i,j-1}}{4}$$
$$\mathrm{CSD}^{\mathrm{strip}}_{i} \approx V_{i} - \frac{V_{i+1}+V_{i-1}}{2}$$

Notably, we did use electrodes that were marked epileptic as reference electrodes if they were neighbouring other electrodes of interest. However, we excluded temporal periods in which an actual epileptic activity was detected. We treated the edges of the lateral grid as 1D strips in order not to lose these data points. CSDs of the four electrodes residing in the corners of the lateral grid were not calculated since they had no neighbouring electrodes on both sides, and similarly for the edges of the occipital strip. After CSD calculation, the signals went through the onset latency estimation procedure described in Section 2.10 'Onset latency estimation'.

2.12 | Gamma-band power calculation

We calculated broadband gamma-band power by high-pass filtering the signals, with 30 Hz cutoff 4th order Butterworth causal filter, and then taking the absolute value of the Hilbert transform and squaring. Importantly, since we were interested in onset latency estimation, we used a causal filter to avoid artificial shift of the onset backward in time. The onset latency of the gamma signal was estimated with the same procedure described in Section 2.10 'Onset latency estimation'.

3 | RESULTS

3.1 | Onset latencies across the posterior cortex

Significant responses and corresponding onset latency estimates (OLEs) were found in 69 out of 112 electrodes (Figure 2 and Supporting information Movie S1). Seven of the 69 electrodes were marked as showing epileptic activity and three more were labelled as 'bad' due to other electrical artefacts (see Section 2 'Materials and methods') and were ignored in the ensuing report of the results. The full list of OLEs is reported in the supporting information (Tables S1.1 and S1.2). Generally, the spatio-temporal distribution of the OLEs followed the expected longer latency with higher hierarchy rank. The earliest OLEs obtained were those of posterior occipital electrodes, around 50–60 ms (but see also Section 3.2 'Very early visual response at posterior intraparietal sulcus'), with relatively little inter-trial variability (see Figure 3 for single trials):

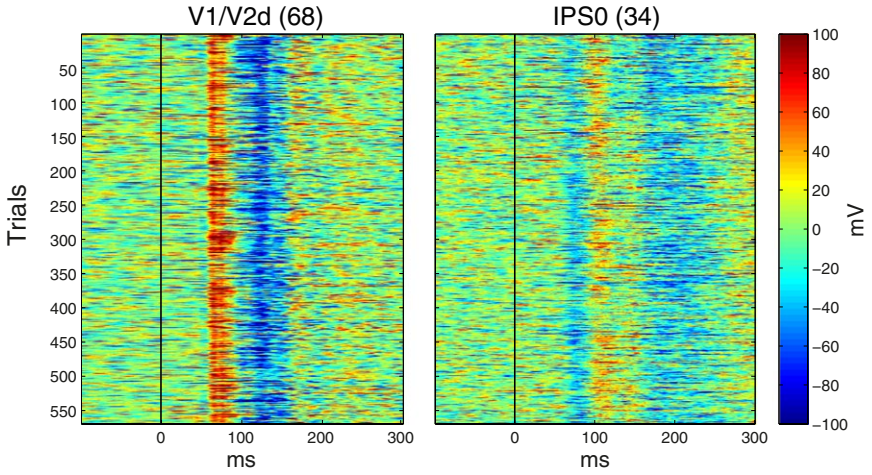

FIGURE 3 Event-related single trials in early responding electrodes. Electrode 68 (left) and electrode 34 (right). Electrodes are labelled due to retinotopic mapping (see Section 2.6 'Co-registration with retinotopic mapping'), as in figures 4 and 5. Note the remarkably consistent onsets in individual trials. [Colour figure can be viewed at wileyonlinelibrary.com]

TABLE 1 Summary of early OLEs at electrodes having retinotopic labels using common average reference (CAR), current source density (CSD) or broadband gamma power

	Reference used		
Electrode localization	**CAR**	**CSD**	**Gamma-band Power**
V1/V2d	50 ± 4	43 ± 3.5	47 ± 2
V1	60 ± 2	60 ± 2	64 ± 5.5
V2d	60 ± 3.5	58 ± 1.5	67 ± 3
V1/V2v	95 ± 3.5	76 ± 30	[b]
V2d/V3d	61 ± 3	[a]	67 ± 2.5
V3v/V2v	170 ± 10	[a]	[b]
IPS0	59 ± 2.5	60 ± 2.5	103 ± 8.5

Notes. Numbers are OLE ± temporal error estimate for the OLE (see Section 2.10 'Onset latency estimation' for further explanation), in milliseconds. Missing electrodes in CSD were excluded from the analysis because they reside on the edge of the occipital strip and therefore are not appropriate for CSD estimation (as explained in Section 2.11 'Current source density (CSD) estimation'). Two electrodes did not have a significant OLE using the broadband gamma power signals.

[a]Electrode excluded from CSD analysis. [b]Electrode did not show a significant OLE.

50 ± 4, 60 ± 2, 60 ± 3.5 and 96 ± 3.5 ms (see Section 3.3 'The early parietal response is not due to volume conduction' for an earlier OLE of the latter electrode using the CSD reference, which emphasizes local activity), in 4 electrodes located over V1 and V2 (see Table 1). All reported OLEs were calculated with a significance level of 0.02 (see Section 2.10 'onset latency estimation'). However, the results are not affected dramatically by varying the significance level of the threshold (Supporting information Figure S2).

We also detected responses and calculated OLEs at various dorsal-parietal and ventral-temporal electrodes, varying between 60 and 200 ms (Figure 2, and see supporting information Table S1.1 for the full list of significant onsets). Generally, the more anterior the electrodes were located, the later the OLEs. However, there were distinctive exceptions to this rule. Electrode 34, located over posterior intraparietal sulcus (IPS) showed a very early response, 59 ± 2.5 ms, a result we return to in more detail in the next section. Another exception was electrode number 55, which had an OLE of 107 ± 6.5 ms, earlier than other electrodes located posterior to it (see Figure 2, lateral and posterior views). A general observation was that electrodes located in the dorsal stream (posterior parietal) responded overall relatively early, within 100 ms, consistent with the view of early processing in the dorsal visual system (Bar, 2006; Bullier, 2001; Chen et al., 2007; Snyder, Shpaner, Molholm, & Foxe, 2012). In contrast, with a few exceptions, most electrodes on the ventral temporal surface responded later, ~100–200 ms OLEs.

Previously, Parvizi et al. (2012), showed a causal and specific role of two electrodes (72, 77 on the middle and posterior fusiform, abbreviated m-fus and p-fus, respectively) in this patient in face perception, by converging results from ECoG, fMRI, and electrical brain stimulation. We report here the OLEs that were obtained for these electrodes: 84 ± 4 ms and 89 ± 4 ms, respectively (Figure 2, supporting information Table S1.1). These electrodes, (together with their neighbour electrode 73) showed the earliest and most reliable onsets among the surrounding electrodes (Figure 2). However, electrode 77 was marked as 'bad' due to electric arteifacts (Figure 2 and Supporting information Table S1.1)

3.2 | Very early visual response at posterior intraparietal sulcus (IPS)

Whereas the general pattern of onset latencies followed the notion of a hierarchy, a significant and robust very early response of 59 ± 2.5 ms was measured in one electrode (no. 34; Figures 2, 3, 4) over the right posterior intraparietal sulcus (IPS) (MNI coordinates −35.12, −78.9, 41.89). fMRI retinotopic mapping placed the electrode over area IPS0 (see Supporting information Figure S4A). We verified that this early visual onset is not due to activity originating from V3A, a relatively low-level visual area (see Supporting information Figure S5). This response onset was nearly simultaneous with the response onset at most striate and peri-striate electrodes that we measured (electrodes 67, 69, 70 which were marked V1, V2d, V2d/V3d, respectively, based on retinotopic mapping, Figure 4 and supporting information Figure S4B). The only earlier responding electrode was electrode number 68, one of the electrodes located over V1/V2d, responding as early as 50 ± 4 ms (Figures 4, 5). Notably, this early response in area V1/V2d is due to a small voltage deflection that was marginally significant (see waveform in Figure 5, for an earlier OLE see also results using CSD in Section 3.3 'The early parietal response is not due to volume conduction'). However, the main voltage deflection of electrode 68 was around 57 ms, nearly simultaneously with other early responding occipital electrodes and the IPS. All electrodes located around electrode 34 had later (or no) OLEs and larger temporal errors

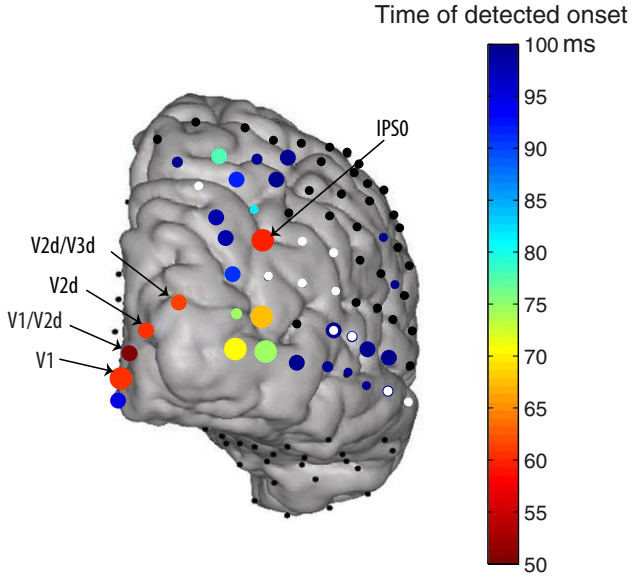

FIGURE 4 Posterior view of early onset latency estimates (OLEs). The same as in Figure 2, but with magnified temporal-scale, see colour bar. Note that onset latencies estimated later than 100 ms are coloured with the darkest blue on the scale. Labels according to retinotopic mapping as in Figure 5 (see Section 2.6 'Co-registration with retinotopic mapping'). Size of the circles is due to temporal error estimate, as in Figure 2. [Colour figure can be viewed at wileyonlinelibrary.com]

(see Figure 4), supporting the claim that the response is localized and specific to the location of electrode 34.

Area MT/V5 is frequently noted in the literature as having a very early onset, comparable to and even earlier than V2 (Bullier, 2001; Ffytche et al., 1995), ascribed to pathways bypassing V1 (Nassi, Lyon, & Callaway, 2006; Sincich, Park, Wohlgemuth, & Horton, 2004). However, the early activation we report is unlikely to coincide with this area. In order to verify this, we localized area MT in the patient's brain in three different ways. First, we converted the Talairach coordinates for MT, which were reported by Dumoulin et al. (2000), to MNI space, using the nonlinear Yale MNI to Talairach coordinate conversion algorithm embedded in BioImage Suite 2.0, http://noodle.med.yale.edu/~papad/mni2tal/, based on Lacadie, Fulbright, Rajeevan, Constable, and Papademetris (2008). We projected these MNI coordinates of MT onto the MNI-normalized brain of the patient. The presumed location of MT/V5 fell at the depth of a sulcus between electrodes 60 and 61 in the lateral grid (see supporting information Section 1 for all electrode numbers on top of the anatomical image). Second, an fMRI-based MT localizer was run on the same patient previously at Stanford Medical Center (unpublished data, courtesy of Dr. Corentin Jacques). Based on activation contrasts between radial grating motion versus static stimuli, the main MT activation was localized closest to electrodes 60–62 and 52–54 (Supporting information Figure S3A), very similar to the localization based on the coordinates reported by Dumoulin et al. (2000). Third, we identified MT by retinotopic maps (Amano, Wandell, & Dumoulin, 2009), in particular, the foveal representation that is distinct from the large foveal confluence of V1–V4. The results were very similar to the previous method (Supporting information Figure S3B). Unlike previous studies using non-invasive source estimation (Ffytche et al., 1995), we did not obtain very early onsets around the presumed location of MT, which is anatomically far from the IPS electrode 34 discussed above. The lack of early visual activity near the presumed MT location might be a consequence of the fact that MT was buried deep in a sulcus, far from any electrode, and due to the stationary stimuli, which were not optimal for activating this region. Notably, consistent with Sunaert, Van Hecke, Marchal, and Orban (1999), some motion-specific fMRI activation was observed, using the motion localizer near the early responding electrode 34 at IPS (see Supporting information Figure S3A).

3.3 | The early parietal response is not due to volume conduction

Since the onsets of most early responding electrodes, including V1 and IPS, were almost simultaneous, it is possible that the IPS electrode actually captured volume-conducted activity from remote occipital electrodes. Several features of the response make this possibility unlikely. First, if the activity was volume conducted, electrodes in between the IPS and the medial occipital cortex should show this conducted activity as well (if not more strongly), but none of them, including other electrodes in the vicinity of IPS showed a similarly early response (see Figure 4).

Second, we repeated the analysis of onset latency estimation in the same way as before, but using the current source density (CSD) event-related waveforms. As noted in the Section 2.11 'Current source density (CSD) estimation', because each electrode is referenced to its neighbours, CSDs are much less sensitive to remote effects than are the CAR measures (Perrin, Bertrand, & Pernier, 1987; and see Figure 5; e.g., electrode 67 was attenuated in CSD versus CAR, presumably due to the filtering out of remote influences). The results of this analysis are shown in Figure 5 and Table 1. IPS electrode 34 still showed early activity (see Figure 5) supporting a robust early localized response at posterior IPS.

One prominent difference in the OLEs obtained, using CSD waveforms compared to CAR, was in the earliest OLE of medial occipital electrode 68 over V1/V2d; an early and small voltage deflection was now detected as significant and resulted in an even earlier OLE, at 43 ± 3.5 ms (see Figure 4). Notably, this early response was significant but small, and still, the major response manifested in a much larger voltage increase around 57 ms (Figure 5).

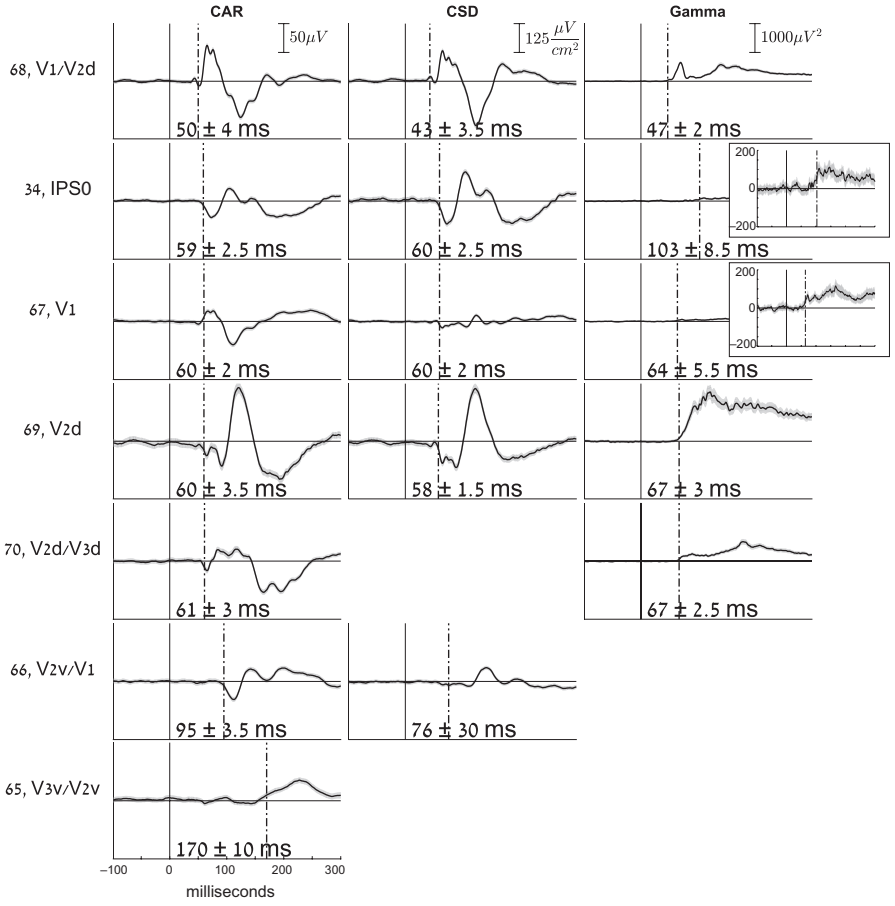

FIGURE 5 Waveforms and onset latency estimates (OLEs). Comparing electrodes having retinotopic labels, using common average reference (CAR), current source density (CSD) or broadband gamma power (Gamma). To the left of each row, the number and retinotopic label of each electrode is specified. For each method, the scale is specified in the first row. Insets for broadband gamma power signals, electrodes 34 and 67, show a magnified y-scale in order to better view the responses. Missing electrodes in CSD were excluded from the analysis because they reside on the edge of the occipital strip and therefore are not appropriate for CSD estimation. Missing electrodes in the broadband gamma power case did not show a significant OLE (see Table 1)

3.4 | Latencies of broadband gamma power

The broadband gamma-band response (as opposed to the narrow-band oscillations elicited by specific stimuli) is considered as a correlate of local asynchronous neuronal firing (Hermes, Nguyen, & Winawer, 2017; Manning, Jacobs, Fried, & Kahana, 2009; Miller et al., 2014; Ray, Maunsell, Fitzgerald, Hsiao, & Johnson, 2011). We calculated the broadband gamma power (30 Hz high-pass cutoff) of all electrodes, and then performed the same onset latency estimation procedure on the power signals (see Section 2.12 'Gamma-band power calculation'). Importantly, we used a causal filter in order not to shift voltage deflections backwards in time. The onsets detected in gamma power signals were generally not earlier than those detected using ERPs (see Supporting information Table S1.3 for all obtained onsets). In the IPS electrode, the power seemed to start increasing around 70 ms postonset. However, this increase only reached significance around 103 ms. See Table 1 and Figure 4 for a comparison of onsets with retinotopic labels, using the three methods (CAR; common average reference, CSD; current source density, or Gamma; gamma-band power signals). See Supporting information Table S1.3 for the full list of OLEs obtained using the gamma-band power signals.

4 | DISCUSSION

The aim of this study was to demonstrate the spatiotemporal evolution of early visual information along the human posterior cortex. By calculating onset latencies using electrocorticographic surface electrodes located at occipital, posterior-temporal and parietal areas, we report the onsets of visual processing at various cortical sites in response to images of objects and faces. Generally, our results show a progression of latencies from early visual cortex along the ventral and dorsal streams of visual processing, as previously demonstrated in monkeys. However, we obtained a very early robust response over the posterior intraparietal sulcus. This early response started around 60 ms, at about the same time that we measure responses over the earliest visual areas. Early access to the dorsal stream was postulated in recent theories of visual processing (Bar, 2006; Bullier, 2001; Chen et al., 2007; Snyder et al., 2012) but direct evidence for such a mechanism in humans is scarce.

According to the JuBrain Cytoarchitectonic atlas viewer (Mohlberg, Eickhoff, Schleicher, Zilles, & Amunts, 2012, https://www.jubrain.fz-juelich.de/apps/cytoviewer/cytoviewer-main.php), using the MNI coordinates of the early IPS electrode, it is located in area PGp of the inferior parietal

cortex, the most caudal area of human IPL. Congruently, the retinotopic mapping in our subject placed the electrode in area IPS0 (supporting information Figure S4A). It is interesting to note that Caspers et al. (2013), found that area PGp contains receptor distributions very similar to those of ventral extrastriate visual cortex. Note, however, that as the electrode is located right over the inferior parietal sulcus in the native patient brain, it could capture as well activity originating from the ventral bank of the sulcus. In the following, we discuss the relationship of our work to previous studies, the possible neuroanatomical pathways leading to the early parietal response, theories of visual processing supporting an early dorsal response, and limitations of our study.

4.1 | Comparison to previous studies

In the monkey, several studies have reported visual onset latencies using invasive electrophysiological measurements. Bullier (2001) reviewed many such studies of single unit recordings in macaque monkeys. In this review, the latencies (medians reported first and then earliest 10% percentile in parenthesis) ranged between 45 and 80 ms (25–45) ms over V1—e.g., 45 (25) ms in Maunsell and Gibson (1992), 55 (40) ms in Knierim and van Essen (1992), 85 (55) ms over V2 (Nowak, Munk, Girard, & Bullier, 1995), 40–75 (45) ms over MT (Raiguel, Xiao, Marcar, & Orban, 1999) and 100 (70) ms over lateral intraparietal (LIP) (Barash, Bracewell, Fogassi, Gnadt, & Andersen, 1991). These latencies are generally longer than those we report here, which can be attributed to the fact that single unit spikes occur later than postsynaptic activity, which governs LFPs and ECoG signals.

A more recent study (Chen et al., 2007) measured laminar field potentials in the macaque, which should be comparable to EEG and ECoG, since they measure average local activity that is correlated with presynaptic activity (Chen et al., 2007; Schroeder et al., 1995). These authors report 31 ms onset latencies over V1 and 33 ms over LIP. Using a rule of thumb of 3/5 ratio of conduction time between the monkey and human (Chen et al., 2007; Schroeder, Molhom, Lakatos, Ritter, & Foxe, 2004), our results compare well to these monkey studies. Ledberg et al. (2007), recording intracortical local field potentials, report longer onset latencies in striate cortex than Chen et al. (2007)(48, 55, and 67 ms in their 3 monkeys). Critically, while their earliest responses were always in the striate cortex, inferior parietal responses were seen within a few ms of the striate cortex, as early or earlier than peristriate cortex, and earlier than superior parietal, or inferior temporal cortex.

Direct evidence for onset latencies of visual responses in humans, with high spatial and temporal resolution, is scarce. In EEG, the C1 ERP component is considered to reflect V1 activity. This is due mainly to the fact that the C1 reverses polarity when the upper and lower visual fields are stimulated, consistent with the "cruciform" representation of these fields on the lower and upper banks of the calcarine sulcus (Clark, Fan, & Hillyard, 1994), although this association has been contested (Ales, Yates, & Norcia, 2010). Based on the C1 scalp component and source estimation, Foxe and Simpson, (2002) found an onset of 56 ms for a presumably V1 source and suggested that later activity was likely driven by a mixture of few more generators. Foxe and Simpson further report that by 70 ms activity is spread over dorso-parietal but not occipito-temporal cortex, which is only active by 80 ms. An earlier EEG study (Ffytche et al., 1995), using motion stimuli, found the earliest activation around 36 ms and more recent MEG studies suggested even earlier response in visual cortex. For example, Inui and colleagues (Inui & Ryusuke, 2006; Inui et al., 2006) and Moradi et al. (2003) using MEG, reported onset times earlier than 30 ms postonset in early visual cortex. Similarly, Shigihara and colleagues (Shigihara & Zeki, 2013, 2014; Shigihara et al., 2016) find significant activity that peaks at around 30–40 ms but starts even earlier. Source reconstruction suggested that activity in this early period extended beyond V1. In one study (Shigihara et al., 2016), activity was found to be significantly above baseline as early as 10–15 ms, although in this case the authors were more hesitant to ascribe this to cortical activity. Indeed, although MEG is arguably superior to EEG in the accuracy of source reconstruction, its resolution and accuracy is nevertheless constrained by the inverse problem.

Due to the proximity of electrodes to the generators, intracranial recordings offer high signal to noise and more precise localization (while providing a more limited spatial coverage). Kirchner, Barbeau, Thorpe, Regis, and Liegeois-Chauvel (2009) measured stereotactic intracranial EEG from an electrode on the superior bank of the calcarine sulcus in humans, and reported onsets around 25 ms. However, onsets were determined by eye rather than by any statistical measure. Yoshor, Bosking, Ghose, and Maunsell (2007), using grids and strips as in the current study, reported the earliest latencies around 56 ms postonset, comparable to the current results, in electrodes presumably over V1–V2. However, they provide only rough localization of their electrodes relative to known visual areas. A rare multiunit recording in humans from two electrodes in area V2–V3 reported onset latencies of just earlier than 60 ms (Self et al., 2016).

Our results, with the advent of precise fMRI retinotopy of the same patient as well as precise electrode localization, show that for meaningful images presented at the center of the visual field as used herein, activity in V1 starts earlier than 50 ms from stimulus onset, and that V2, as well as parietal sources, are also activated by 60 ms (Table 1), and hence may contribute to the early VEP (e.g., to the C1 component).

It is hard to directly compare, or to make a strong statement, about the absolute latency of the earliest response in visual cortex. As noted, the numbers in humans range from

as early as 10–15 ms, to 60+ ms. This divergence very likely results from cardinal differences in the stimulation, the filtering parameters, and the statistical criteria for determining onsets. For example, intracellular recording of the nonhuman primate retina shows slower responses in the fovea than in the periphery, probably due different cone kinetics (Sinha et al., 2017), and, congruently, cortical responses from nonhuman primates (Schroeder et al., 1998) show that activation is faster for more peripheral than more central stimuli. In addition, larger stimuli would likely also produce earlier response simply by virtue of activating more neurons. Indeed, the results reviewed above showing very early activity in humans of 30 ms or earlier used stimuli like large checkerboard placed away from fixation, or even full field flashes. The luminance of the stimulus, and the degree of adaptation of retinal and cortical cells, is likely to affect the speed in which activation would be measureable as well. For example, the above-mentioned studies by Inui et al. (Inui & Ryusuke, 2006; Inui et al., 2006), which reported responses earlier than 30 ms, used strong, full field flashes, after dark adapting their subjects for about 15 min. The content of the image may affect latencies as well, probably due to low level difference like spatial frequencies. For example, examining figure 7 in Kirchner et al.'s study (Kirchner et al., 2009) suggests an earlier onset for checkerboard than for scenes in the human FEF. The method used to determine onset responses is also critical. Some studies use more lenient criteria, like eyeballing, to determine onsets, while others use more conservative and controlled methods like the permutation method used here, which would delay the determined onset. Thus, as noted before (Shigihara et al., 2016), the relative activation latency of different areas within subject and paradigm seems to be of more interest than absolute latencies. In that sense, despite the different absolute latencies, our study is congruent with the previous conclusions from the MEG and EEG studies reviewed above, showing near simultaneous activation of striate and specific extra-striate cortex, as departure from a strictly hierarchical feedforward organization (cf. Zeki, 2016). Specifically, our results points to very early activity in the IPS.

Chambers, Payne, Stokes, and Mattingley (2004), using TMS, showed that the right angular gyrus is involved in reorienting attention during two discrete temporal periods: early (90–120 ms) and late (210–240 ms) after target onset. Since our IPS electrode 34 was located right over the sulcus, it might reflect responses originating in both banks of the IPS. If the origin of the response is on the ventral bank of IPS (i.e., the angular gyrus), then the early IPS onset that we measured might be functionally related to the early period of attention orientation in Chambers et al.'s study, since the measured ERP waveform at the IPS indeed onsets at 59 ms but unfolds between 60 and 100 ms approximately, commensurate with Chambers et al.'s early period.

4.2 | Neuroanatomical origin of the early parietal response

How does visual stimulation reach the early IPS source so early? One possibility is that the IPS response is driven by direct projections from subcortical structures, bypassing V1. These V1-bypassing pathways are widely discussed in the context of 'blindsight'—a neuropsychological condition in which, despite damage to primary visual cortex, some visual abilities are preserved (Barbur, Watson, Frackowiak, & Zeki, 1993; Weiskrantz, Warrington, Sanders, & Marshall, 1974). The sub-cortical structures projecting directly to extra-striate cortex can be either the thalamic lateral geniculate nucleus (LGN), or pulvinar nucleus (PN), reviewed recently by (Zeki, 2016). The other possibility is that very early responses in V1 are relayed directly to the IPS via feed-forward connections. Because we based our calculations on stimulus-locked averages, and the stimulus onset time was nonpredictable, it is not probable that top-down connections drive this response directly (although top-down connections might alter sustained excitability and hence encourage earlier onsets). Next, we discuss these putative sources.

The LGN receives most of its input directly from parvo and magnocellular ganglion cells of the retina, although some inputs also pass via the superior colliculus (SC) (for a review, see Leopold, 2012). Projections from LGN to cortical areas other than V1 were demonstrated directly in the monkey. For example, Sincich et al. (2004) found a direct projection from LGN to area MT/V5 in the macaque using retrograde tracing. Others reported visually driven fMRI activation in several extastriate areas in V1-lesioned macaques, including V2,V3,V4, V5/MT, and lateral intraparietal area (LIP) (Schmid et al., 2010). fMRI activation in all these sites, as well as behavioural detection of the visual target, was suppressed following reversible inactivation of the LGN. This provides a strong support for LGN being the source of the residual activation, although it does not determine whether the LGN was the direct source for any of the activated loci, nor it determines the latencies of the activity in the extrastriate regions. In humans, Bridge, Thomas, Jbabdi, and Cowey (2008) showed evidence for an ipsilateral structural pathway between LGN and area MT/V5 in both blindsight patient and controls, using diffusion-weighted MRI. These findings support the existence of direct pathways from LGN to area MT/V5, other extrastriate regions, and perhaps parietal areas as well, bypassing V1. However, whether this pathway is fast enough to deliver signals into the IPS as early as 60 ms, is unknown. It was suggested that direct projections from LGN to the extrastriate and parietal cortex originate from koniocellular cells located at the intercalated layers of LGN (Hendry & Reid, 2000). Most koniocellular (K) projections are small and have thin axons (Reese & Guillery, 1987), and thus should have slower conduction velocities than the magnocellular

projections to V1. This suggests that the koniocellular pathway is an unlikely candidate for explaining the fast parietal response we measured. However, some studies suggest that K cells are very heterogeneous morphologically and physiologically (Hendry & Reid, 2000; Leopold, 2012; Schiller & Malpeli, 1977).

Visual information can also enter the cortex bypassing V1 via the PN. The PN gets input through the retino-tectal pathway, via the SC. The retino-tectal pathway has long been thought of as linked functionally to the dorsal stream in regulating spatial attention, control of eye movements and visually driven behaviour (Petersen, Robinson, & Morris, 1987; Rafal, Henik, & Smith, 1991; Sapir, Soroker, Berger, & Henik, 1999), which seem to require fast access of visual information. Indeed, it was lately established that a colliculo-pulvinar pathway projects to extrastriate cortex directly; Lyon, Nassi, and Callaway (2010) found a disynaptic pathway from SC to extra-striate cortex, passing through PN and from there to dorsal stream areas MT and V3 (but not to V2 or V4). Moreover, direct retinal afferent projections also innervate the same PN subdivision (inferior pulvinar nucleus, PIm), which projects to area MT, as recently found in the marmoset (Leopold, 2012; Warner, Goldshmit, & Bourne, 2010), and this pathway may provide fast cortical activation. Although there is no clear evidence for PN projections to parietal areas, considering the association of both the retino-tectal pathway and the inferior parietal cortex to spatial attention, this pathway may be involved in the fast responses we observed.

Finally, it is also possible that the early parietal response stems from the earliest responses measured in V1, which are relayed to the IPS via feed-forward connections. We measured a very early response at a single electrode located over V1/V2d (electrode 68), as early as 50 ± 4 ms using CAR, and even 43 ± 3.5 using CSD. Notably, this very early activity reflects a small voltage deflection in the ERP (see Figure 4) while the following, and much larger response in the same electrode, as well as activity in all other striate and peri-striate electrodes onsets at approximately the same time as IPS, around 60 ms. It could still be the case that by the time that activation in V1 and peri-striate areas becomes strong, the earliest weaker responses have already been carried forward and arrived to parietal cortex. Such mechanisms have been postulated before (Chen et al., 2007; VanRullen & Thorpe, 2002), and the notion of 'single spike wave propagation' was even used for modeling of neural latency codes for vision that can account for fast visual performance (Kirchner et al., 2009; Thorpe, Delorme, & Van Rullen, 2001; VanRullen & Thorpe, 2002). Importantly, this fast transfer of information from V1 to IPS in about 10–15 ms would require 1 or 2 synapses in between them. According to (Felleman & Van Essen, 1991), in macaques there is a direct connection between V1 and posterior parietal area (PIP) as well as from V2 to PIP, but not from V1-2 to lateral intraparietal (LIP). To our knowledge, there is no direct evidence for such connections in humans.

4.3 | Very early visual processing in the dorsal stream

The early parietal response onset we report here is in accordance with current theories of visual information processing in the brain, as well as with empirical evidence. For instance, Chen et al. (2007) show dorsal-to-ventral stream latency advantage at several stages of the processing hierarchy in monkeys. Considering the functional role of the dorsal stream in spatial vision (Mishkin, Ungerleider, & Macko, 1983), and in attending to locations in space, these lateral connections could serve to prepare the ventral system for further processing at a given location. Several theoretical claims were raised stressing the need for early access of relatively crude information to the visual system, serving to guide and prepare it for more detailed and efficient later processing (Bar, 2006; Bullier, 2001; Chen et al., 2007; Snyder et al., 2012). Bullier (2001) reviews evidence for early visual responses in primate parietal and frontal cortex belonging to the dorsal visual stream, which he calls all-together 'the fast brain'. He postulates the importance of these fast responses in interacting with and modulating lower order visual areas for integration of global-to-local visual information via feedback connections. Similarly, the 'frame-and-fill' model suggests that object recognition is achieved by gradually integrating fine details into an already established whole (Bar, 2006; Snyder et al., 2012). According to this view, structures in the dorsal visual stream have an important role in initial parsing of the stimulus and passing it on to prefrontal and ventral areas, which then bit by bit process further specific details. Our results provide the first direct electrophysiological evidence for very early parietal, dorsal stream response in the human brain, which is essentially assumed in all the discussed models.

4.4 | Limitations and conclusion

The current results are based on a single subject. One of the limitations of using ECoG is that electrode type and location are determined based on clinical needs and it is therefore hard to find another patient having electrodes located over the exact same areas. It is especially rare to find an ECoG patient having electrodes implanted over striate areas (for an example, in more than 300 cases recorded by the group of RTK, one of the authors of the present study, less than a handful had electrodes covering V1), and even more rare is to find a patient with both striate and parietal electrodes, who also went through retinotopic mapping. Other groups may have access to similar data, and the current case report should stimulate attempts to replicate the findings in appropriate patients' data.

The electrode grids are located on the surface of the cortex, and cover about 10 functional columns, or roughly $2–5 \times 10^5$ neurons. Consequently, some neural responses may be missed if they are too weak, farther away from the electrode, or if the spatial orientation of the responding neuronal population in the tissue under the electrode is such that dipoles cancel each other. Another reason for possibly missing earlier responses is the analysis itself. Our onset latency estimation analysis is designed to bind the type I error (false alarms). There is no assurance that the test is sensitive enough to detect the earliest responses if they are weak relative to the noise.

It is also the case that the illumination of pixels on an LCD screen is gradual, and the exact luminance level at which retinal responses are elicited is undetermined. Further, our dependent measure was a change in the evoked potential and broadband power. It is possible that other measures like single unit spiking or denser electrode arrays could show shorter latencies. Interestingly, the power of the broadband (gamma) response emerged later than the evoked response, especially in the IPS electrode. These differences stress the functional distinction between these two types of signals, as has been observed previously in the spatial domain (Winawer et al., 2013). However, the evoked potentials and the broadband response have been associated with synaptic input potentials and local neural spiking, respectively, the relationship between these two signals is yet to be elucidated.

Another limitation stems from the process of determining the precise location of the ECoG electrodes on the cortex anatomically. Our methods, like most other ECoG studies, depend on co-registration of CT image depicting the electrodes, with an anatomical MRI scan that was done prior to electrode placement. The alignment of these images is not trivial, both because of difference between the imaging modalities and the fact that the brain itself might move a bit during the surgery. While several methods have been developed in order to overcome these limitations (e.g., Dykstra et al., 2012; Hermes et al., 2010), the localization of electrodes should be taken with some error margin. For an example, we cannot be sure whether electrode 34 was located more over the ventral or dorsal banks of the intraparietal sulcus.

Nevertheless, considering the roughly 5:3 ratio between human and monkey latencies, respectively, due to size differences (Chen et al., 2007; Schroeder et al., 2004), the latencies we find are consistent with the reports from the monkey using penetrating electrodes and single unit recordings. Despite the discussed limitations, to our knowledge this is the first direct report of the onset timing of visual processing across multiple spatially localized sites in the human cortex, and specifically for the very early parietal response. Additional such measurements are needed for establishment of the generality of these results and for further exact characterization of the timing of early visual processing in the human cortex. Analysis schemes as devised here can easily be applied to existing bulks of ECoG data recorded for other purposes, for systematic examination of the onsets of processing in various cortical areas.

ACKNOWLEDGEMENTS

The authors are grateful to Dr. Josef Parvizi for facilitating ECoG data collection from his patient and for fruitful discussions about the results. We acknowledge Vinitha Rangarajan and Bret Foster for assisting with data collection at the Stanford Medical Center. We thank Corentin Jacques for generously sharing with us the ECoG MT localizer data that he collected on the patient. We thank Israel Nelken for valuable consultations. This work was supported by grant 2013070 from the United States-Israel Binational Science Foundation to LYD and RTK and grant 1902_2014 from the Israel Science Foundation to LYD as well as NIH grant R01MH111417 to JW. Leon Y. Deouell is supported by the Jack A. Skirball research fund. TIR was supported by The Hoffman Leadership and Responsibility Fellowship Program at the Hebrew University of Jerusalem.

CONFLICT OF INTEREST

The authors declare that they have no conflict of interest.

AUTHOR CONTRIBUTIONS

Conceptualization, L.Y.D. and T.I.R; Methodology, T.I.R and L.Y.D; Formal Analysis, T.I.R, J.W. and E.M.G; Resources, R.T.K.; Writing – Original Draft, T.I.R.; Writing – Review and Editing, L.Y.D., J.W. and R.T.K.; Visualization, T.I.R. and J.W.; Supervision, L.Y.D.; Funding Acquisition, L.Y.D., R.T.K and, J.W.

DATA ACCESSIBILITY

All analysis scripts and data are publicly available (https://doi.org/10.17605/osf.io/x3e9r). For any further requests, please contact the corresponding authors.

ORCID

Tamar I. Regev http://orcid.org/0000-0003-0639-0890
Jonathan Winawer http://orcid.org/0000-0001-7475-5586
Leon Y. Deouell http://orcid.org/0000-0002-6147-5208

REFERENCES

Ales, J. M., Yates, J. L., & Norcia, A. M. (2010). V1 is not uniquely identified by polarity reversals of responses to upper and lower visual

field stimuli. *NeuroImage*, *52*, 1401–1409. https://doi.org/10.1016/j.neuroimage.2010.05.016

Amano, K., Wandell, B. A., & Dumoulin, S. O. (2009). Visual field maps, population receptive field sizes, and visual field coverage in the human MT+ complex. *Journal of Neurophysiology*, *102*, 2704–2718. https://doi.org/10.1152/jn.00102.2009

Bar, M. (2006). Top down facilitation of visual recognition. *Proceedings of the National Academy of Sciences of the USA*, *103*, 449–454. https://doi.org/10.1073/pnas.0507062103

Barash, S., Bracewell, R. M., Fogassi, L., Gnadt, J. W., & Andersen, R. A. (1991). Saccade-related activity in the lateral intraparietal area. I. Temporal properties; comparison with area 7a. *Journal of Neurophysiology*, *66*, 1095–1108. https://doi.org/10.1152/jn.1991.66.3.1095

Barbur, J. L., Watson, J. D., Frackowiak, R. S., & Zeki, S. (1993). Conscious visual perception without V1. *Brain*, *116*(Pt 6), 1293–1302. https://doi.org/10.1093/brain/116.6.1293

Bridge, H., Thomas, O., Jbabdi, S., & Cowey, A. (2008). Changes in connectivity after visual cortical brain damage underlie altered visual function. *Brain*, *131*, 1433–1444. https://doi.org/10.1093/brain/awn063

Bullier, J. (2001). Integrated model of visual processing. *Brain Research. Brain Research Reviews*, *36*, 96–107. https://doi.org/10.1016/S0165-0173(01)00085-6

Butler, J. S., Molholm, S., Fiebelkorn, I. C., Mercier, M. R., Schwartz, T. H., & Foxe, J. J. (2011). Common or redundant neural circuits for duration processing across audition and touch. *Journal of Neuroscience*, *31*, 3400–3406. https://doi.org/10.1523/JNEUROSCI.3296-10.2011

Carvalhaes, C., & de Barros, J. A. (2015). The surface Laplacian technique in EEG: Theory and methods. *International Journal of Psychophysiology*, *97*, 174–188. https://doi.org/10.1016/j.ijpsycho.2015.04.023

Caspers, S., Schleicher, A., Bacha-Trams, M., Palomero-Gallagher, N., Amunts, K., & Zilles, K. (2013). Organization of the human inferior parietal lobule based on receptor architectonics. *Cerebral Cortex*, *23*, 615–628. https://doi.org/10.1093/cercor/bhs048

Chambers, C. D., Payne, J. M., Stokes, M. G., & Mattingley, J. B. (2004). Fast and slow parietal pathways mediate spatial attention. *Nature Neuroscience*, *7*, 217–218. https://doi.org/10.1038/nn1203

Chen, C.-M., Lakatos, P., Shah, A. S., Mehta, A. D., Givre, S. J., Javitt, D. C., & Schroeder, C. E. (2007). Functional anatomy and interaction of fast and slow visual pathways in macaque monkeys. *Cerebral Cortex*, *17*, 1561–1569. https://doi.org/10.1093/cercor/bhl067

Clark, V. P., Fan, S., & Hillyard, S. A. (1994). Identification of early visual evoked potential generators by retinotopic and topographic analyses. *Human Brain Mapping*, *2*, 170–187. https://doi.org/10.1002/hbm.460020306

Dumoulin, S. O., Bittar, R. G., Kabani, N. J., Baker, C. L., Le Goualher, G., Pike, B. G., & Evans, A. C. (2000). A new anatomical landmark for reliable identification of human area V5/MT: A quantitative analysis of sulcal patterning. *Cerebral Cortex*, *10*, 454–463. https://doi.org/10.1093/cercor/10.5.454

Dumoulin, S. O., & Wandell, B. A. (2008). Population receptive field estimates in human visual cortex. *NeuroImage*, *39*, 647–660. https://doi.org/10.1016/j.neuroimage.2007.09.034

Dykstra, A. R., Chan, A. M., Quinn, B. T., Zepeda, R., Keller, C. J., Cormier, J., … Cash, S. S. (2012). Individualized localization and cortical surface-based registration of intracranial electrodes. *NeuroImage*, *59*, 3563–3570. https://doi.org/10.1016/j.neuroimage.2011.11.046

Felleman, D. J., & Van Essen, D. C. (1991). Distributed hierarchical processing in the primate cerebral cortex. *Cerebral Cortex*, *1*, 1–47. https://doi.org/10.1093/cercor/1.1.1

Ffytche, D. H., Guy, C. N., & Zeki, S. (1995). The parallel visual motion inputs into areas V1 and V5 of human cerebral cortex. *Brain*, *118*(Pt 6), 1375–1394. https://doi.org/10.1093/brain/118.6.1375

Foxe, J. J., & Simpson, G. V. (2002). Flow of activation from V1 to frontal cortex in humans. A framework for defining "early" visual processing. *Experimental Brain Research*, *142*, 139–150. https://doi.org/10.1007/s00221-001-0906-7

Gerber, E. M., Golan, T., Knight, R. T., & Deouell, L. Y. (2017). Cortical representation of persistent visual stimuli. *NeuroImage*, *161*, 67–79. https://doi.org/10.1016/j.neuroimage.2017.08.028

Hendry, S. H. C., & Reid, R. C. (2000). The Koniocellular pathway In primate vision. *Annual Review of Neuroscience*, *1*, 127–153. https://doi.org/10.1146/annurev.neuro.23.1.127

Hermes, D., Miller, K. J., Noordmans, H. J., Vansteensel, M. J., & Ramsey, N. F. (2010). Automated electrocorticographic electrode localization on individually rendered brain surfaces. *Journal of Neuroscience Methods*, *185*, 293–298. https://doi.org/10.1016/j.jneumeth.2009.10.005

Hermes, D., Nguyen, M., & Winawer, J. (2017). Neuronal synchrony and the relation between the blood-oxygen-level dependent response and the local field potential. *PLoS Biology*, *15*, e2001461. https://doi.org/10.1371/journal.pbio.2001461

Hjorth, B. (1975). An on-line transformation of EEG scalp potentials into orthogonal source derivations. *Electroencephalography and Clinical Neurophysiology*, *39*, 526–530. https://doi.org/10.1016/0013-4694(75)90056-5

Inui, K., & Ryusuke, K. (2006). Temporal analysis of the flow from V1 to the extrastriate cortex in humans. *Journal of Neurophysiology*, *96*, 775–784. https://doi.org/10.1152/jn.00103.2006

Inui, K., Sannan, H., Miki, K., Kaneoke, Y., & Kakigi, R. (2006). Timing of early activity in the visual cortex as revealed by simultaneous MEG and ERG recordings. *NeuroImage*, *30*, 239–244. https://doi.org/10.1016/j.neuroimage.2005.09.003

Jenkinson, M., Bannister, P., Brady, M., & Smith, S. (2002). Improved optimization for the robust and accurate linear registration and motion correction of brain images. *NeuroImage*, *17*, 825–841. https://doi.org/10.1006/nimg.2002.1132

Jenkinson, M., & Smith, S. (2001). A global optimisation method for robust affine registration of brain images. *Medical Image Analysis*, *5*, 143–156. https://doi.org/10.1016/S1361-8415(01)00036-6

Keren, A. S., Yuval-Greenberg, S., & Deouell, L. Y. (2010). Saccadic spike potentials in gamma-band EEG: Characterization, detection and suppression. *NeuroImage*, *49*, 2248–2263. https://doi.org/10.1016/j.neuroimage.2009.10.057

Kirchner, H., Barbeau, E. J., Thorpe, S. J., Regis, J., & Liegeois-Chauvel, C. (2009). Ultra-rapid sensory responses in the human frontal eye field region. *Journal of Neuroscience*, *29*, 7599–7606. https://doi.org/10.1523/JNEUROSCI.1233-09.2009

Knierim, J. J., & van Essen, D. C. (1992). Neuronal responses to static texture patterns in area V1 of the alert macaque monkey. *Journal of Neurophysiology*, *67*, 961–980. https://doi.org/10.1152/jn.1992.67.4.961

Lacadie, C. M., Fulbright, R. K., Rajeevan, N., Constable, R. T., & Papademetris, X. (2008). More accurate Talairach coordinates for neuroimaging using non-linear registration. *NeuroImage*, *42*, 717–725. https://doi.org/10.1016/j.neuroimage.2008.04.240

Ledberg, A., Bressler, S. L., Ding, M., Coppola, R., & Nakamura, R. (2007). Large-scale visuomotor integration in the cerebral cortex. *Cerebral Cortex*, *17*, 44–62. https://doi.org/10.1093/cercor/bhj123

Leopold, D. A. (2012). Primary visual cortex: Awareness and blindsight. *Annual Review of Neuroscience*, *35*, 91–109. https://doi.org/10.1146/annurev-neuro-062111-150356

Lyon, D. C., Nassi, J. J., & Callaway, E. M. (2010). A disynaptic relay from superior colliculus to dorsal stream visual cortex in macaque monkey. *Neuron*, *65*, 270–279. https://doi.org/10.1016/j.neuron.2010.01.003

Manning, J. R., Jacobs, J., Fried, I., & Kahana, M. J. (2009). Broadband shifts in local field potential power spectra are correlated with single-neuron spiking in humans. *Journal of Neuroscience*, *29*, 13613–13620. https://doi.org/10.1523/JNEUROSCI.2041-09.2009

Maunsell, J. H., & Gibson, J. R. (1992). Visual response latencies in striate cortex of the macaque monkey. *Journal of Neurophysiology*, *68*, 1332–1344. https://doi.org/10.1152/jn.1992.68.4.1332

Miller, K. J., Honey, C. J., Hermes, D., Rao, R. P., denNijs, M., & Ojemann, J. G. (2014). Broadband changes in the cortical surface potential track activation of functionally diverse neuronal populations. *NeuroImage*, *85*, 711–720. https://doi.org/10.1016/j.neuroimage.2013.08.070

Mishkin, M., Ungerleider, L. G., & Macko, K. A. (1983). Object vision and spatial vision: Two cortical pathways. *Trends in Neurosciences*, *6*, 414–417. https://doi.org/10.1016/0166-2236(83)90190-X

Mohlberg, H., Eickhoff, S., Schleicher, A., Zilles, K., & Amunts, K. (2012). *A new processing pipeline and release of cytoarchitectonic probabilistic maps—JuBrain*. OHBM: Beijing, China.

Moradi, F., Liu, L. C., Cheng, K., Waggoner, R. A., Tanaka, K., & Ioannides, A. A. (2003). Consistent and precise localization of brain activity in human primary visual cortex by MEG and fMRI. *NeuroImage*, *18*, 595–609. https://doi.org/10.1016/S1053-8119(02)00053-8

Nassi, J. J., Lyon, D. C., & Callaway, E. M. (2006). The parvocellular LGN provides a robust disynaptic input to the visual motion area MT. *Neuron*, *50*, 319–327. https://doi.org/10.1016/j.neuron.2006.03.019

Nowak, L. G., Munk, M. H. J., Girard, P., & Bullier, J. (1995). Visual latencies in areas V1 and V2 of the macaque monkey. *Visual Neuroscience*, *12*, 371–384. https://doi.org/10.1017/S095252380000804X

Parvizi, J., Jacques, C., Foster, B. L., Withoft, N., Rangarajan, V., Weiner, K. S., & Grill-Spector, K. (2012). Electrical stimulation of human fusiform face-selective regions distorts face perception. *Journal of Neuroscience*, *32*, 14915–14920. https://doi.org/10.1523/JNEUROSCI.2609-12.2012

Perrin, F., Bertrand, O., & Pernier, J. (1987). Scalp current density mapping: Value and estimation from potential data. *IEEE Transactions on Biomedical Engineering*, *34*, 283–288. https://doi.org/10.1109/TBME.1987.326089

Petersen, S. E., Robinson, D. L. E. E., & Morris, J. D. (1987). Contributions of the pulvinar to visual spatial attention. *Neuropsychologia*, *25*, 97–105. https://doi.org/10.1016/0028-3932(87)90046-7

Rafal, R., Henik, A., & Smith, J. (1991). Extrageniculate contributions to reflex visual orienting in normal humans: A temporal hemifield advantage. *Journal of Cognitive Neuroscience*, *3*, 322–328. https://doi.org/10.1162/jocn.1991.3.4.322

Raiguel, S. E., Xiao, D. K., Marcar, V. L., & Orban, G. A. (1999). Response latency of macaque area MT/V5 neurons and its relationship to stimulus parameters. *Journal of Neurophysiology*, *82*, 1944–1956. https://doi.org/10.1152/jn.1999.82.4.1944

Ray, S., Maunsell, J. H. R., Fitzgerald, P. J., Hsiao, S. S., & Johnson, K. O. (2011). Different origins of gamma rhythm and high-gamma activity in macaque visual cortex. *PLoS Biology*, *9*, e1000610.

Reese, B. E., & Guillery, R. W. (1987). Distribution of axons according to diameter in the monkey's optic tract. *Journal of Comparative Neurology*, *260*, 453–460. https://doi.org/10.1002/(ISSN)1096-9861

Sapir, A., Soroker, N., Berger, A., & Henik, A. (1999). Inhibition of return in spatial attention: Direct evidence for collicular generation. *Nature Neuroscience*, *2*, 1053–1054. https://doi.org/10.1038/15977

Schiller, P. H., & Malpeli, J. G. (1977). Properties and tectal projections of monkey retinal ganglion cells. *Journal of Neurophysiology*, *40*, 428–445. https://doi.org/10.1152/jn.1977.40.2.428

Schmid, M. C., Mrowka, S. W., Turchi, J., Saunders, R. C., Wilke, M., Peters, A. J., … Leopold, D. A. (2010). Blindsight depends on the lateral geniculate nucleus. *Nature*, *466*, 373–377. https://doi.org/10.1038/nature09179

Schmolesky, M. T., Wang, Y., Hanes, D. P., Thompson, K. G., Leutgeb, S., Schall, J. D., & Leventhal, A. G. (1998). Signal timing across the macaque visual system. *Journal of Neurophysiology*, *79*, 3272–3278. https://doi.org/10.1152/jn.1998.79.6.3272

Schroeder, C. E., Mehta, A. D., & Givre, S. J. (1998). A spatiotemporal profile of visual system activation revealed by current source density analysis in the awake macaque. *Cerebral Cortex*, *8*, 575–592. https://doi.org/10.1093/cercor/8.7.575

Schroeder, C. E., Molhom, S., Lakatos, P., Ritter, W., & Foxe, J. (2004). Human-simian correspondence in the early cortical processing of multisensory cues. *Cognitive Processing*, *5*, 140–151.

Schroeder, C., Steinschneider, M., Javitt, D., Tenke, C., Givre, S., Mehta, A., … Vaughan, H. (1995). Localization of ERP generators and identification of underlying neural processes. In G. Karmos, M. Molnar, V. Csepe, I. Czigler, & J. E. Desmedt (Eds.), *Perspectives of event- related potentials in research (EEG Suppl 44)* (pp. 55–75). Amsterdam, The Netherlands: Elsevier.

Self, M. W., Peters, J. C., Possel, J. K., Reithler, J., Goebel, R., Ris, P., … Roelfsema, P. R. (2016). The effects of context and attention on spiking activity in human early visual cortex. *PLoS Biology*, *14*, e1002420. https://doi.org/10.1371/journal.pbio.1002420

Shigihara, Y., Hoshi, H., & Zeki, S. (2016). Early visual cortical responses produced by checkerboard pattern stimulation. *NeuroImage*, *134*, 532–539. https://doi.org/10.1016/j.neuroimage.2016.03.078

Shigihara, Y., & Zeki, S. (2013). Parallelism in the brain's visual form system. *European Journal of Neuroscience*, *38*, 3712–3720. https://doi.org/10.1111/ejn.12371

Shigihara, Y., & Zeki, S. (2014). Parallel processing of face and house stimuli by V1 and specialized visual areas: A magnetoencephalographic (MEG) study. *Frontiers in Human Neuroscience*, *8*, 901.

Sincich, L. C., Park, K. F., Wohlgemuth, M. J., & Horton, J. C. (2004). Bypassing V1: A direct geniculate input to area MT. *Nature Neuroscience*, *7*, 1123–1128. https://doi.org/10.1038/nn1318

Sinha, R., Hoon, M., Baudin, J., Okawa, H., Wong, R. O. L., & Rieke, F. (2017). Cellular and circuit mechanisms shaping the perceptual properties of the primate fovea. *Cell*, *168*(413–426), e412.

Snyder, A. C., Shpaner, M., Molholm, S., & Foxe, J. J. (2012). Visual object processing as a function of stimulus energy, retinal eccentricity and Gestalt configuration: A high-density electrical mapping study. *Neuroscience*, *221*, 1–11. https://doi.org/10.1016/j.neuroscience.2012.03.035

Sunaert, S., Van Hecke, P., Marchal, G., & Orban, G. A. (1999). Motion-responsive regions of the human brain. *Experimental Brain Research*, *127*, 355–370. https://doi.org/10.1007/s002210050804

Thorpe, S., Delorme, A., & Van Rullen, R. (2001). Spike-based strategies for rapid processing. *Neural Networks*, *14*, 715–725. https://doi.org/10.1016/S0893-6080(01)00083-1

VanRullen, R., & Thorpe, S. J. (2002). Surfing a spike wave down the ventral stream. *Vision Research*, *42*, 2593–2615. https://doi.org/10.1016/S0042-6989(02)00298-5

Wandell, B. A., & Winawer, J. (2011). Imaging retinotopic maps in the human brain. *Vision Research*, *51*, 718–737. https://doi.org/10.1016/j.visres.2010.08.004

Wang, L., Mruczek, R. E. B., Arcaro, M. J., & Kastner, S. (2014). Probabilistic maps of visual topography in human cortex. *Cerebral Cortex*, *25*, 3911–3931.

Warner, C. E., Goldshmit, Y., & Bourne, J. A. (2010). Retinal afferents synapse with relay cells targeting the middle temporal area in the pulvinar and lateral geniculate nuclei. *Frontiers in Neuroanatomy*, *4*, 8.

Weiskrantz, L., Warrington, E. K., Sanders, M. D., & Marshall, J. (1974). Visual capacity in the hemianopic field following a restricted occipital ablation. *Brain*, *97*, 709–728. https://doi.org/10.1093/brain/97.1.709

Winawer, J., Horiguchi, H., Sayres, R. A., Amano, K., & Wandell, B. A. (2010). Mapping hV4 and ventral occipital cortex: The venous eclipse. *Journal of Vision*, *10*, 1–1. https://doi.org/10.1167/10.5.1

Winawer, J., Kay, K. N., Foster, B. L., Rauschecker, A. M., Parvizi, J., & Wandell, B. A. (2013). Asynchronous broadband signals are the principal source of the BOLD response in human visual cortex. *Current Biology*, *23*, 1145–1153. https://doi.org/10.1016/j.cub.2013.05.001

Yoshor, D., Bosking, W. H., Ghose, G. M., & Maunsell, J. H. (2007). Receptive fields in human visual cortex mapped with surface electrodes. *Cerebral Cortex*, *17*, 2293–2302. https://doi.org/10.1093/cercor/bhl138

Zeki, S. (2016). Multiple asynchronous stimulus- and task-dependent hierarchies (STDH) within the visual brain's parallel processing systems. *European Journal of Neuroscience*, *44*, 2515–2527. https://doi.org/10.1111/ejn.13270

SUPPORTING INFORMATION

Additional supporting information may be found online in the Supporting Information section at the end of the article.

How to cite this article: Regev TI, Winawer J, Gerber EM, Knight RT, Deouell LY. Human posterior parietal cortex responds to visual stimuli as early as peristriate occipital cortex. *Eur J Neurosci*. 2018;48:3567–3582. https://doi.org/10.1111/ejn.14164